Intracellular calcium movements during relaxation and recovery of superfast muscle fibers of the toadfish swimbladder

Frank E. Nelson,[1,3,4] Stephen Hollingworth,[2] Lawrence C. Rome,[1,3] and Stephen M. Baylor[2]

[1]Department of Biology and [2]Department of Physiology, Perelman School of Medicine, University of Pennsylvania, Philadelphia, PA 19104
[3]Whitman Center, The Marine Biological Laboratory, Woods Hole, MA 02543
[4]Department of Biology, Temple University, Philadelphia, PA 19122

The mating call of the Atlantic toadfish is generated by bursts of high-frequency twitches of the superfast twitch fibers that surround the swimbladder. At 16°C, a calling period can last several hours, with individual 80–100-Hz calls lasting ∼500 ms interleaved with silent periods (intercall intervals) lasting ∼10 s. To understand the intracellular movements of Ca^{2+} during the intercall intervals, superfast fibers were microinjected with fluo-4, a high-affinity fluorescent Ca^{2+} indicator, and stimulated by trains of 40 action potentials at 83 Hz, which mimics fiber activity during calling. The fluo-4 fluorescence signal was measured during and after the stimulus trains; the signal was also simulated with a kinetic model of the underlying myoplasmic Ca^{2+} movements, including the binding and transport of Ca^{2+} by the sarcoplasmic reticulum (SR) Ca^{2+} pumps. The estimated total amount of Ca^{2+} released from the SR during a first stimulus train is ∼6.5 mM (concentration referred to the myoplasmic water volume). At 40 ms after cessation of stimulation, the myoplasmic free Ca^{2+} concentration ($[Ca^{2+}]$) is below the threshold for force generation (∼3 µM), yet the estimated concentration of released Ca^{2+} remaining in the myoplasm ($\Delta[Ca_M]$) is large, ∼5 mM, with ∼80% bound to parvalbumin. At 10 s after stimulation, $[Ca^{2+}]$ is ∼90 nM (three times the assumed resting level) and $\Delta[Ca_M]$ is ∼1.3 mM, with 97% bound to parvalbumin. Ca^{2+} movements during the intercall interval thus appear to be strongly influenced by (a) the accumulation of Ca^{2+} on parvalbumin and (b) the slow rate of Ca^{2+} pumping that ensues when parvalbumin lowers $[Ca^{2+}]$ near the resting level. With repetitive stimulus trains initiated at 10-s intervals, Ca^{2+} release and pumping come quickly into balance as a result of the stability (negative feedback) supplied by the increased rate of Ca^{2+} pumping at higher $[Ca^{2+}]$.

The Journal of General Physiology

INTRODUCTION

The superfast fibers that surround the swimbladder of the Atlantic toadfish (*Opsanus tau*) are the fastest-contracting vertebrate fibers known (Rome, 2006). They generate the fish's mating call by vibrating the walls of the gas-filled swimbladder at a high frequency (80–200 Hz; 15–25°C). To do so, the fibers contract and relax at the frequency of the sound, and the one-to-one relation between muscle twitches and the production of sound pulses makes it possible, by use of a hydrophone, to study superfast fiber function remotely during undisturbed animal behaviors (Elemans et al., 2014). These fibers are also a source of important anatomical and biochemical information about the molecular components of excitation-contraction coupling associated with the membranes of the transverse tubules and SR (Appelt et al., 1991; Feher et al., 1998; Felder and Franzini-Armstrong, 2002). Because these fibers have many unusual adaptations that allow them to function at high frequencies, they provide an exceptional model system for the study of Ca^{2+} cycling during normal muscle activity.

Recently, Harwood et al. (2011) estimated the amount of Ca^{2+} that is released from the SR when a superfast fiber is stimulated to give a high-frequency train of action potentials (APs) and twitches that mimics fiber activity during a mating call. The estimates are based on two independent experimental approaches: (1) measurements of recovery oxygen consumption in the presence of the cross-bridge blocker *N*-benzyl-*p*-toluene sulphonamide (BTS) and (2) modeling of SR Ca^{2+} release based on measurements of the change in the myoplasmic-free Ca^{2+} concentration ($\Delta[Ca^{2+}]$) with furaptra, a low-affinity rapidly responding fluorescent Ca^{2+} indicator.

Because toadfish can call repetitively for many hours, it is also of interest to estimate the movements of Ca^{2+} in the recovery periods between sound production. Typically, individual mating calls last ∼0.5 s and are interleaved with a silent period (the "intercall interval"), which lasts ∼10 s. One important question addressed in this article is whether all of the SR Ca^{2+} that is released during a mating call is returned to the SR by the end of the

Correspondence to Stephen M. Baylor: baylor@mail.med.upenn.edu

Abbreviations used in this paper: AP, action potential; BTS, *N*-benzyl-*p*-toluene sulphonamide; EDL, extensor digitorum longus; FDHM, full duration at half maximum.

The Rockefeller University Press $30.00
J. Gen. Physiol. Vol. 143 No. 5 605–620
www.jgp.org/cgi/doi/10.1085/jgp.201411160

intercall interval. To understand such Ca^{2+} movements, we have injected individual superfast fibers with fluo-4, a high-affinity Ca^{2+}-selective indicator, and measured the indicator's fluorescence signal during and after high-frequency stimulus trains that mimic fiber activity during calling (e.g., 40 APs at 83 Hz; 16°C). A kinetic model was then used to simulate the fluo-4 signal and thereby quantify the Ca^{2+} movements on a time scale of seconds. On this slow time scale, the primary movements are those involved with the return of Ca^{2+} to the SR by the activity of the SR Ca^{2+} pump molecules and the unbinding of Ca^{2+} from parvalbumin.

The measurements and simulations indicate that, after a single 40-AP stimulus train at 83 Hz, it takes at least 60 s for Ca^{2+} to be fully returned to the SR. If repetitive calling is mimicked with a series of stimulus trains initiated at 10-s intervals, the results indicate that (a) at 10 s after the first train, ∼20% of the released Ca^{2+} has not yet been returned to the SR by Ca^{2+} pumping; (b) the amount of Ca^{2+} released in trains after the first is 80–85% of that released in the first train; and (c) release and pumping come quickly into balance in trains after the first because of a rise in baseline $[Ca^{2+}]$ and the associated increased rate of Ca^{2+} pumping. Repetitive high-frequency activity of a fiber can therefore continue as long as the overall metabolic state of the cell remains energized.

MATERIALS AND METHODS

Ethical approval

Animal protocols were approved by the Institutional Animal Care and Use Committee of the University of Pennsylvania.

Experimental measurements

The experiments were performed at 16°C with methods similar to those described previously (Rome et al., 1996; Harwood et al., 2011). A toadfish was sacrificed and a small bundle of swimbladder fibers was isolated by dissection in a fish Ringer's solution that contained (mM): 132 NaCl, 2.6 KCl, 1 $MgCl_2$, 2.7 $CaCl_2$, 10 imidazole, and 10 sodium pyruvate, pH 7.7. Seven toadfish were used for the experiments, with measurements made from one or two fiber bundles per fish. Each bundle was mounted in an experimental chamber on an optical bench apparatus equipped for measuring changes in fluorescence intensity in response to AP stimulation. To minimize movement artifacts in the fluorescence records, the bundle was stretched to a sarcomere length of 2.7–3.1 µm. In most experiments, 5 µM BTS was also included in the Ringer's solution, which further reduced fiber movement (Cheung et al., 2002). The potassium-salt form of fluo-4 (Life Technologies) was introduced into the myoplasm of one fiber on the surface of the bundle by pressure injection. Fluo-4's resting fluorescence (F_R) and changes during activity (ΔF) were measured from a 300-µm length of fiber located 0.3–1 mm from the site of indicator injection. The band pass of the excitation and emission wavelengths were 450–490 nm and ≥510 nm, respectively. The mean concentration of fluo-4 at the measurement site was ∼50 µM (Table 1).

ΔF was elicited by a propagating AP or a train of APs set up by point-wise stimulation from a pair of extracellular electrodes located adjacent to the bundle surface near the injection site. Only fibers that responded with an all-or-nothing ΔF signal were used for experimentation. Where possible, the ΔF signal was normalized by F_R, which was estimated in a two-step procedure. First, the raw measurement of resting fluorescence was corrected for the intrinsic fluorescence of the bundle, which contributes to the measured resting intensity but is not related to the presence of fluo-4. The intrinsic fluorescence was estimated from a region of the bundle that did not contain the indicator and subtracted from the raw fluorescence to give F_R of the fiber. Second, because the fiber F_R arises from the indicator in both the "central core" (Appelt et al., 1991) and the myofibrillar region of the fiber, F_R was divided by 1.46 to obtain the estimate of F_R in the myofibrillar region (Harwood et al., 2011). The latter step was taken because ΔF is thought to arise primarily from the myofibrillar region, and the model simulations (see next section) consider Ca^{2+}-related changes, including fluo-4's $\Delta F/F_R$ signal, in the myofibrillar region only. Unfortunately, it was not possible to make an accurate estimate of F_R in all experiments. This situation arose because (a) the diameter of superfast swimbladder fibers is small, 26 ± 2 µm (mean ± SEM; range 15–35 µm; $n = 9$), (b) the amount of fluo-4 injected into the fibers was small so as to avoid concentrations of indicator that would have a substantial buffering effect on $\Delta[Ca^{2+}]$, and (c) fluo-4 is largely Ca^{2+} free in a resting fiber, and thus its fluorescence intensity is low. As a result, in several experiments, the raw value of resting fluorescence was only slightly larger than the estimated intrinsic fluorescence of the bundle. In this circumstance, F_R, and hence the amplitude of $\Delta F/F_R$, became uncertain even though the ΔF signal itself could usually be recorded with a large signal-to-noise ratio. The calibration of the $\Delta F/F_R$ signal was not considered reliable unless the estimate of fiber F_R was at least 50% of that of the intrinsic fluorescence of the bundle. Even with this criterion, the individual values of F_R, and thus the amplitude of $\Delta F/F_R$, may have uncertainties as large as ∼25%.

Baseline correction of the ΔF signals

To track the time course of $[Ca^{2+}]$'s return to the resting level after activity, several of the fluo-4 ΔF signals were recorded for

TABLE 1

Myoplasmic concentrations of the modeled constituents in swimbladder fibers

Constituent	Concentration	Concentration of binding sites
	µM	*µM*
Resting free $[Ca^{2+}]$	0.030	
Resting free $[Mg^{2+}]$	1,000	
Troponin	106	212 (Ca^{2+} regulatory sites)
Parvalbumin	2,670	5,340 (Ca^{2+}/Mg^{2+} sites)
SR Ca^{2+} pump	980	1,960 (Ca^{2+} transport sites)
ATP	8,000	8,000 (Ca^{2+}/Mg^{2+} sites)
Fluo-4	50	50 (Ca^{2+} sites)
Protein	3,000	3,000 (fluo-4 sites)

All concentrations are spatially averaged and refer to the myoplasmic water volume in the myofibrillar region; except for free $[Ca^{2+}]$ and free $[Mg^{2+}]$, total concentrations are given. The concentrations are taken from Harwood et al. (2011), except for free $[Ca^{2+}]$, fluo-4, and protein (see Model simulations). The concentration of protein applies to the four-state reaction scheme between fluo-4 and protein (Table 2, E). The mean concentration of fluo-4 was estimated from comparisons of fluo-4's resting fluorescence in swimbladder fibers with the concentration and resting fluorescence of fluo-3 estimated in singly dissected frog twitch fibers (Harkins et al., 1993; Hollingworth et al., 2000, 2001), with appropriate adjustments made for differences in fiber diameters. The fluo-3 concentration estimates in frog fibers are thought to be quite accurate because measurements of both indicator absorbance and fluorescence were made in these fibers (Harkins et al., 1993), and fiber diameters can be measured accurately in frog fibers.

many seconds after cessation of stimulation. All ΔF signals of this type were corrected for a small drift in baseline fluorescence that was recorded over an identical time period but in the absence of stimulation. The exact source of this baseline drift is not known with certainty, but one contributing factor is the (net) diffusion of indicator along the fiber axis, into or out of the field of optical recording. This factor varies with the amount of indicator injected, the time of injection, and the distance of the recording site from the injection site. The baseline drift, which was measured immediately before and/or immediately after all active records of long duration, was approximately linear in time. A straight line was fitted to the baseline drift and subtracted from the associated active record, thereby yielding the baseline-corrected ΔF signal. Because, at the end of a long sweep, the amplitude of the baseline drift was always a small fraction (<0.01) of the peak amplitude of the corresponding active signal, the baseline-correction procedure has virtually no effect on the properties estimated for the peak of the signal.

Model simulations

The major intracellular Ca^{2+} movements in the myofibrillar region of the fiber were estimated with a single-compartment (spatially averaged) kinetic model. Table 1 gives the concentrations of the myoplasmic constituents included in the model, and Table 2 gives the modeled reactions and their rate constants. The selection of the basic model parameters is explained in Harwood et al. (2011), with some changes for this study noted below. The concentration of all variables is referred to the myoplasmic water volume in the myofibrillar region.

A simulation begins when an assumed flux of SR Ca^{2+} enters the myoplasm in the myofibrillar region. A set of first-order differential equations is then used to calculate the associated changes in the following time-dependent variables: $\Delta[Ca^{2+}]$, Δ[CaDye] (the change in concentration of Ca^{2+} bound to fluo-4), and the change in concentration of Ca^{2+} bound to the intrinsic myoplasmic Ca^{2+} buffers, including troponin (Δ[CaTrop]), ATP (Δ[CaATP]), parvalbumin (Δ[CaParv]), and the SR Ca^{2+} pumps (Δ[CaPump]). The amount of Ca^{2+} returned to the SR by Ca^{2+} pumping (Δ[CaPumped]) is also calculated. The time integral of the release flux gives $\Delta[Ca_T]$, the total concentration of Ca^{2+} released from the SR, which also equals $\Delta[Ca^{2+}] + \Delta$[CaDye] + Δ[CaTrop] + Δ[CaATP] + Δ[CaParv] + Δ[CaPump] + Δ[CaPumped].

For the current study, three changes were made to the modeling parameters. First, the forward and reverse rate constants for the binding reactions between Ca^{2+} and the Ca^{2+} pump (Table 2, D, first two reactions) were doubled. This change was made to agree with the kinetic parameters for the Ca^{2+} pump used in recent simulations in mouse and frog twitch fibers (Hollingworth et al., 2012; Hollingworth and Baylor, 2013), which are also thought to be reasonable for swimbladder fibers (Young et al., 2003). With this change, the estimate of $\Delta[Ca_T]$ elicited by an AP is ∼10% larger than that calculated in the original model 3 of Harwood et al. (2011) (see the first section of Results).

The second change was made because the myoplasmic Ca^{2+} transients were monitored with fluo-4 rather than furaptra. Table 2 (E) gives the four-state reaction scheme used to model fluo-4's behavior in the myoplasm, which is assumed to be like that deduced previously for fluo-3 (Harkins et al., 1993). The relative fluorescence intensities of the four states of fluo-4 are also assumed to be like those of fluo-3, namely Dye, 1; CaDye, 200; PrDye, 2; and CaPrDye, 200 (Baylor et al., 2002). With these values and with the reaction scheme in Table 2 (E) and the concentrations of fluo-4 and protein in Table 1, the equilibrium relation between $[Ca^{2+}]$ and fluo-4's fluorescence intensity is closely mimicked by a 1:1 binding reaction in which the intensity of fluo-4 at saturating $[Ca^{2+}]$ divided by that at zero $[Ca^{2+}]$ is 106 and the effective dissociation constant of fluo-4 for Ca^{2+} is 2.20 µM. This value of the dissociation constant in myoplasm reflects the fact that (a) with fluo-based indicators, a large fraction (0.8–0.9) of the indicator appears to be bound to myoplasmic proteins and (b) the Ca^{2+} dissociation constant of protein-bound fluo is three- to fourfold larger than that of protein-free fluo (Table 2; Harkins et al., 1993).

The third change involved a reduction in myoplasmic resting $[Ca^{2+}]$, 30 nM (Table 1) rather than 50 nM. This change was made to slow somewhat the simulated return of $\Delta[Ca^{2+}]$ to baseline on a time scale of seconds and thereby give better agreement with the measured fluo-4 $\Delta F/F_R$ signal on this slow time scale. The 30 nM value is at the low end of the range estimated for resting $[Ca^{2+}]$ in intact twitch fibers from frog muscle (30–45 nM, *Rana pipiens*; Hollingworth et al., 2001). It should be emphasized that the main conclusions from the simulations about the intracellular movements of Ca^{2+} in swimbladder fibers on a time scale of seconds are not altered by the exact value chosen for resting $[Ca^{2+}]$ or for several other model parameters that can also be adjusted to produce a slower return of $\Delta[Ca^{2+}]$ to baseline, e.g., a smaller concentration of Ca^{2+} pump molecules (Feher et al., 1998) or slower rate constants in the kinetic scheme of the Ca^{2+} pump (Harwood et al., 2011; see also Fig. 10 described in Results).

The rate of SR Ca^{2+} release elicited by an AP is assumed to satisfy an empirical equation defined by rising and falling exponentials (Baylor and Hollingworth, 1998, 2007):

$$\begin{aligned}&\text{Release rate}(t) = 0 \text{ if } t < T,\\ &= R \cdot \left[1 - \exp\left(-(t-T)/\tau 1\right)\right]^5 \cdot \exp\left(-(t-T)/\tau 2\right) \text{ if } t \geq T.\end{aligned} \quad (1)$$

In the case of a rested fiber, R associated with one AP (or the first AP of a stimulus train) was chosen so that $\Delta[Ca_T]$ is 750 µM (Harwood et al., 2011). The time-shift parameter T simulates the delay between the external shock that generates the AP and the onset of Ca^{2+} release; its value (2–5 ms) was adjusted so that the rising phase of the simulated ΔF waveform matched that of the measurement. $\tau 1$ and $\tau 2$ were set to 0.80 ms and 0.32 ms, respectively, so as to yield a release waveform whose full duration at half maximum (FDHM) is 1.0 ms (Harwood et al., 2011). Ca^{2+} releases elicited by the second and subsequent APs of a stimulus train were assumed to follow the same functional form except that (a) each value of R was adjusted so that the corresponding peak of ΔF in the simulated waveform approximately matched that in the measurement and (b) each value of T was increased appropriately to reflect the time of stimulation of the corresponding AP. The success of the simulations was evaluated by comparing the overall time course of the simulated and measured $\Delta F/F_R$ waveforms. The simulations were performed with the mathematical modeling program MLAB (Civilized Software Inc.).

Statistical analysis

Statistical tests were performed in MLAB with Student's two-tailed t test. Results were considered significant if $P < 0.05$.

RESULTS

Estimation of $\Delta[Ca^{2+}]$ and SR Ca^{2+} release with furaptra in superfast swimbladder fibers

In previous experiments at 16°C (Rome et al., 1996; Harwood et al., 2011), the properties of Ca^{2+} transients in toadfish swimbladder fibers were determined in response to stimulation with either a single AP or a high-frequency train of APs. In these experiments, $\Delta[Ca^{2+}]$ was measured with furaptra, a low-affinity kinetically rapid Ca^{2+} indicator, so the properties of $\Delta[Ca^{2+}]$ are reasonably well known. In response to one AP, the 10–100% rise

time, peak amplitude, and FDHM of $\Delta[Ca^{2+}]$ are estimated to be ~1.8 ms, ~30 µM, and ~3.0 ms, respectively. With a high-frequency stimulus at 83 Hz, the $\Delta[Ca^{2+}]$ signals elicited by APs after the first also have a brief time course, but their peak amplitudes are only 20–40% of that caused by the first AP.

Analysis of the furaptra Ca^{2+} transients with a single-compartment model like that described in Materials and methods permitted estimation of several important physiological variables, including (a) the change in concentration of troponin molecules whose Ca^{2+} regulatory sites are doubly occupied with Ca^{2+}($\Delta[Ca_2Trop]$), i.e., the troponin molecules that most directly influence force generation, (b) the total concentration of Ca^{2+} that is released from the SR ($\Delta[Ca_T]$), and (c) the rate of SR Ca^{2+} release (calculated as $(d/dt)\Delta[Ca_T]$).

With one AP, the estimated peak of $\Delta[Ca_2Trop]$ is ~85 µM, which corresponds to ~80% of the troponin molecules being in the Ca_2Trop state (Harwood et al., 2011). With later APs in a high-frequency train, the estimated peaks of $\Delta[Ca_2Trop]$ are smaller, as expected from the smaller peaks of $\Delta[Ca^{2+}]$ and the fast kinetics of the Ca^{2+}-troponin reaction, and $\Delta[Ca_2Trop]$ returns close to baseline between stimuli. The decline in $\Delta[Ca_2Trop]$

TABLE 2

Reactions and rate constants for the modeled constituents in swimbladder fibers (16°C)

Reaction	Forward rate (k_{on})	Reverse rate (k_{off})	Ratio (k_{off}/k_{on})
		s^{-1}	μM
A			
$Ca^{2+} + ATP \leftrightarrow CaATP$	$1.5 \times 10^8\ M^{-1}s^{-1}$	30,000	200
$Mg + ATP \leftrightarrow MgATP$	$1.5 \times 10^6\ M^{-1}s^{-1}$	150	100
B			
$Ca^{2+} + Parv \leftrightarrow CaParv$	$1.25 \times 10^8\ M^{-1}s^{-1}$	1.5	0.012
$Mg + Parv \leftrightarrow MgParv$	$1.00 \times 10^5\ M^{-1}s^{-1}$	9	91.0
C			
$Ca^{2+} + Trop \leftrightarrow CaTrop$	$0.885 \times 10^8\ M^{-1}s^{-1}$	345	3.9
D			
$Ca^{2+} + E \leftrightarrow CaE$	$1.74 \times 10^8\ M^{-1}s^{-1}$	6.96	0.04
$Ca^{2+} + CaE \leftrightarrow Ca_2E$	$1.74 \times 10^8\ M^{-1}s^{-1}$	8.70	0.05
$Mg + E \leftrightarrow MgE$	$8.70 \times 10^4\ M^{-1}s^{-1}$	4.35	50
$Mg + MgE \leftrightarrow Mg_2E$	$8.70 \times 10^4\ M^{-1}s^{-1}$	87.0	1,000
$H + E \leftrightarrow HE$	Instantaneous	Instantaneous	(pK = 8)
$H + HE \leftrightarrow H_2E$	Instantaneous	Instantaneous	(pK = 8)
$H + H_2E \leftrightarrow H_3E$	Instantaneous	Instantaneous	(pK = 6)
$H + H_3E \leftrightarrow H_4E$	Instantaneous	Instantaneous	(pK = 5)
$Ca_2E \leftrightarrow E + (2\ Ca)$	$3.48\ s^{-1}$	0	0
E			
$Ca^{2+} + Dye \leftrightarrow CaDye$	$2.33 \times 10^8\ M^{-1}s^{-1}$	179	0.77
$Pr + Dye \leftrightarrow PrDye$	$0.100 \times 10^8\ M^{-1}s^{-1}$	3,670	367
$Ca^{2+} + PrDye \leftrightarrow CaPrDye$	$0.150 \times 10^8\ M^{-1}s^{-1}$	43.0	2.87
$Pr + CaDye \leftrightarrow CaPrDye$	$0.100 \times 10^8\ M^{-1}s^{-1}$	13,800	1,380

The first column gives the reaction steps and the second and third columns the reaction rate constants for ATP (A), parvalbumin (B), the regulatory sites on troponin (C), the SR Ca^{2+} pump (D, where E denotes Enzyme), and the indicator dye fluo-4 (E). The fourth column gives the dissociation constants of the reactions (k_{off}/k_{on}). In A, the indicated rate constants are for $[K^+]$ = 150 mM, pH = 7, and viscosity = 2 centipoise (Baylor and Hollingworth, 1998). In B, the parvalbumin rate constants are those in model 3 of Harwood et al. (2011). In C, the two regulatory sites on each troponin molecule are assumed to be independent and have identical reaction rate constants with Ca^{2+} (Rome et al., 1996). In D, the reaction steps are adapted from the scheme of Peinelt and Apell (2002), with dissociation constants involving protons expressed as pKs (shown in parentheses); the parentheses on the right-hand side of the last reaction in column 1 denote the two Ca^{2+} ions transported to the lumen of the SR with each reaction cycle. In E, "Pr" denotes protein sites capable of binding fluo-4 (Table 1). The fluo-4 reaction scheme is the same as that for fluo-3 (Harkins et al., 1993); the rate constants are derived from the values given by Hollingworth et al. (2000) for fluo-3 in frog myoplasm at 16°C in combination with information from Woodruff et al. (2002) about the Ca^{2+} dissociation constants ($K_{d,Ca}$) of fluo-3 and fluo-4 in a simple salt solution. The latter article reports that the values of $K_{d,Ca}$ of fluo-3 and fluo-4 are similar, with a similar temperature dependence; the extrapolated value of $K_{d,Ca}$ at 16°C is 0.8–0.9 µM for both indicators. Harkins et al. (1993) reported a somewhat smaller $K_{d,Ca}$ for fluo-3 in a simple salt solution at 16°C, 0.51 µM. The value of $K_{d,Ca}$ for protein-free fluo-4 given above (0.77 µM) was selected to fall within the range reported for fluo-3 and fluo-4 by Harkins et al. (1993) and Woodruff et al. (2002). The reaction rate constants of fluo-4 (second and third columns) are based on those of Hollingworth et al. (2000) for fluo-3 and the assumption that a larger value of $K_{d,Ca}$ arises from a larger off-rate constant. At the resting values of free $[Ca^{2+}]$ (30 nM), free $[Mg^{2+}]$ (1 mM), and pH (7), the resting fractional occupancies of the different states of the various model constituents are as follows: (A) ATP (0.909), MgATP (0.091), CaATP (0.000); (B) Parv (0.070), CaParv (0.173), MgParv (0.758); (C) Trop (0.992), CaTrop (0.008); (D) E (0.006), CaE (0.004), Ca_2E (0.002), MgE (0.123), Mg_2E (0.123), HE (0.062), H_2E (0.617), H_3E (0.062), H_4E (0.001); (E) Dye (0.109), CaDye (0.004), PrDye (0.878), CaPrDye (0.009). The model assumes that the rate of Ca^{2+} pumping in the resting state, ~0.01 µM/ms, is balanced by an equivalent (and constant) leak of Ca^{2+} from the SR into the myoplasm.

between stimuli is consistent with observations from tension recordings on bundles of swimbladder fibers in which active tension returns close to baseline between the individual stimuli in a high-frequency train (Rome et al., 1996).

The peak amplitude and FDHM of the SR Ca^{2+} release waveform in response to one AP are estimated to be ~600 μM/ms and ~1.0 ms, respectively, and $\Delta[Ca_T]$ is estimated to be 750–800 μM. With subsequent APs in a high-frequency stimulus, the releases occur with a similarly brief time course, but the release amounts are, on average, only 20–40% of the first release. This large decline in release is thought to be primarily caused by the process of Ca^{2+} inactivation of Ca^{2+} release (Harwood et al., 2011). These estimates of the release amounts were confirmed in parallel experiments in which recovery oxygen consumption was measured on bundles of swimbladder fibers exposed to the cross-bridge blocker BTS and activated by high-frequency stimuli of various durations (15°C; Harwood et al., 2011).

The fluo-4 $\Delta F/F_R$ signal elicited by an AP

To study Ca^{2+} movements during relaxation and recovery, it is advantageous to use a Ca^{2+} indicator such as fluo-4 that has a relatively high affinity for Ca^{2+} and good selectivity over Mg^{2+}. Fig. 1 A shows an example of the $\Delta F/F_R$ signal elicited by an AP in a superfast fiber injected with fluo-4. Because the fiber was well immobilized, the $\Delta F/F_R$ signal is likely to be free (or almost free) of movement artifacts. The 10–100% rise time, peak amplitude, and FDHM are 2.5 ms, 25.8, and 14.0 ms, respectively. Because of fluo-4's high affinity, it is expected (e.g., Baylor and Hollingworth [2011]) that the rise time and FDHM of $\Delta F/F_R$ are longer than the corresponding values for $\Delta[Ca^{2+}]$ estimated with furaptra (1.8 ms and 3.0 ms, respectively; previous section). Similar values of 10–100% rise time, peak amplitude, and FDHM of the fluo-4 signal elicited by an AP were seen in several experiments (Table 3, A, first column).

Fig. 1 B shows the trace from Fig. 1 A displayed on a time scale of seconds, which is relevant to the recovery processes after a call, and at a 25-fold higher vertical gain. Also shown is the fit of a decaying exponential function to the $\Delta F/F_R$ signal beginning 1 s after stimulation (declining dashed trace; described below). By 60 s, the $\Delta F/F_R$ signal has returned close to baseline (horizontal dashed line), but a small offset, <1% of the peak signal, remains. Similar small offsets were seen in all experiments of this type (Table 3, B, first column, last row). It is not known whether the small maintained signal at 60 s is caused by a small residual elevation of $[Ca^{2+}]$ above the resting level (e.g., of ~10 nM; estimated with the scheme in Table 2, E) or is caused by some unknown change in fluo-4 not directly related to $[Ca^{2+}]$. An explanation of this property of the late fluo-4 ΔF signal is not considered essential for the issues addressed in this paper, which relate primarily to Ca^{2+} movements during the ~10-s intercall interval (see below). Interestingly, the maintained signal is not unique to swimbladder fibers, as small maintained increases in $\Delta F/F_R$ at 60 s after an AP are also seen in other types of fibers injected with fluo-4 or fluo-3, including frog twitch fibers, mouse fast-twitch fibers, and mouse slow-twitch fibers (unpublished data). A similar maintained signal, consistent with a small elevation in $[Ca^{2+}]$, is also seen in frog twitch fibers injected with fura-2 (18°C; Suda and Kurihara, 1991).

The fluo-4 signal elicited by a high-frequency train of APs

In five experiments, the fluo-4 signal was measured on a 60-s time base in a well-immobilized fiber that was activated by a train of 40 APs at 83 Hz, a stimulus used to mimic one call of the toadfish's repetitive mating call. Fig. 2 shows results from two of these experiments. In the experiment of Fig. 2 (A and B), F_R could be reasonably estimated, and this fluo-4 signal is shown in units of $\Delta F/F_R$. In the other experiments of this type, including the experiment of Fig. 2 (C and D), F_R could not be

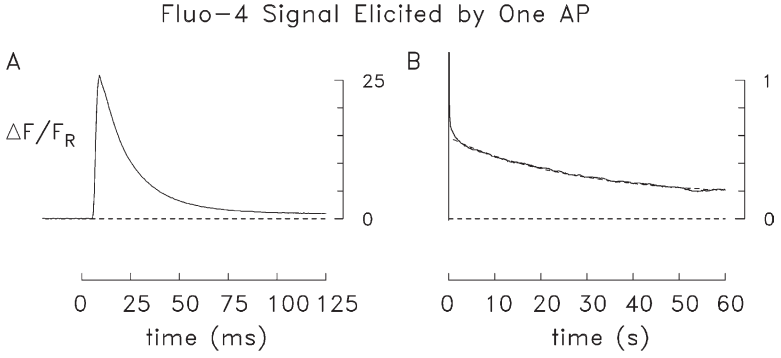

Figure 1. Example of the fluo-4 $\Delta F/F_R$ signal elicited by an AP in a well-immobilized superfast swimbladder fiber (16°C). (A) At zero time, the fiber was stimulated by an external shock. The 10–100% rise time, peak amplitude, and FDHM of $\Delta F/F_R$ are 2.5 ms, 25.8, and 14.0 ms, respectively. The trace is a single sweep (i.e., no signal averaging was used). For the calibration of the fluo-4 signal, F_R refers here, and throughout Results, to the indicator's fluorescence intensity in the myofibrillar region of the fiber (see Materials and methods). (B) Same trace as in A but displayed on a higher gain and slower sweep speed. The declining dashed trace (which is poorly visible) shows a least-squares fit to the measurement between 1 and 60 s based on a decaying single-exponential function plus a baseline offset, with the following fitted values: exponential time constant, 26.5 s; exponential amplitude, 0.411; and baseline offset, 0.160. Fiber number 072612.2.

reliably estimated because of interference from the intrinsic fluorescence of the fiber bundle and the generally small myoplasmic concentrations of fluo-4 in the experiments (see Materials and methods). For this reason, the signals in Fig. 2 (C and D) are displayed normalized to ΔF_1 (defined as the peak amplitude of the fluorescence change elicited either by one AP or by the first AP in a stimulus train or by the first AP in a series of stimulus trains). It is reasonable to believe that the amplitude of $\Delta F_1/F_R$ in this experiment and in the other experiments of this type averaged 25–30, i.e., was similar to that in Figs. 1 A and 2 A and to the mean peak $\Delta F/F_R$ in the first column of Table 3 (A), 28.7. In Fig. 2 (A and C), each ΔF trace reveals 40 individual peaks, 1 for each stimulated AP. The amplitude of the ΔF peaks after the first reach a value that is either slightly larger than ΔF_1 (Fig. 2 A) or slightly smaller than ΔF_1 (Fig. 2 C). Similar results were seen in the five experiments of this type, with the ΔF peaks after the first being slightly smaller than, similar to, or slightly larger than ΔF_1.

After cessation of stimulation, the ΔF signals in Fig. 2 (A and C) decayed within ~100 ms to a quasi-steady level that is 30–40% of that of ΔF_1. Between 600 and 1,000 ms, the ΔF signals declined only slightly. Similar results were seen in the other experiments of this type. The time constant describing the early decay of ΔF to the quasi-steady level averaged 24 ± 4 ms (mean ± SEM; $n = 7$).

Fig. 2 (B and D) shows the ΔF signals of Fig. 2 (A and C) displayed on a 60-s time base and at fivefold higher vertical gain. These traces have also been fitted with a decaying exponential function during the time 1–60 s after stimulation (declining dashed traces; described in the next section). As in Fig. 1, the experimental traces in Fig. 2 (B and D) are elevated above baseline at 60 s, when $\Delta F/\Delta F_1$ is 0.02 and 0.04, respectively. In experiments of this type, the mean value (±SEM) of $\Delta F/\Delta F_1$ at 60 s was 0.024 ± 0.005 ($n = 7$; Table 3, B, second column, last entry). As mentioned in the preceding section, the source of this maintained signal, if not caused by $\Delta[Ca^{2+}]$, is unknown.

Quantitative characterization of the decay of the fluo-4 signal on a time scale of seconds

As noted above, on a time scale of 60 s, the fluo-4 ΔF signal decays slowly and incompletely (Figs. 1 and 2). Because fluo-4 is a high-affinity Ca^{2+}-selective indicator, the time course of this decay is likely to largely reflect the time course with which $[Ca^{2+}]$ declines toward the resting level. To provide an empirical characterization of the decay of the fluo-4 signal, the $\Delta F/\Delta F_1$ waveforms elicited by either a single AP or a train of 40 APs at 83 Hz were fitted from 1 to 60 s by a decaying exponential function to a baseline offset (see, e.g., declining dashed traces in Fig. 1 B and Fig. 2 [B and D]). With one AP, a single-exponential decay to an offset gave a good fit to the measurements; with the 83-Hz train of APs, a double-exponential decay to an offset was required for a good fit. Table 3 (C) gives the mean parameter values obtained in these fits. The time-dependent components in these fits likely reflect (a) the declining rate with which Ca^{2+} is pumped by the SR Ca^{2+} pumps as $[Ca^{2+}]$ approaches the resting level (see simulations described below), (b) the net rate at which Ca^{2+} dissociates from parvalbumin at low $[Ca^{2+}]$ (see also simulations), and

TABLE 3

Properties of fluo-4 signals in toadfish swimbladder fibers (16°C)

Parameter	1 AP (mean ± SEM; *n*)	40 APs at 83 Hz (mean ± SEM; *n*)
A: Early signal		
10–100% rise time (ms)	2.6 ± 0.1; 10	–
Peak $\Delta F/F_R$	28.7 ± 2.0; 5	–
FDHM (ms)	15.1 ± 0.5; 10	–
B: Late signal amplitudes		
$\Delta F(1\ s)/\Delta F_1$	0.030 ± 0.003; 5	0.263 ± 0.014; 7
$\Delta F(60\ s)/\Delta F_1$	0.009 ± 0.003; 5	0.024 ± 0.005; 7
C: Fitted values, 1–60 s		
A1 ($\Delta F/F_1$)	0.021 ± 0.002; 5	0.119 ± 0.011; 7
$\tau 1$ (s)	23.3 ± 2.5; 5	1.85 ± 0.10; 7
A2 ($\Delta F/F_1$)	–	0.112 ± 0.008; 7
$\tau 2$ (s)	–	10.7 ± 0.9; 7
Offset ($\Delta F/F_1$)	0.007 ± 0.004; 5	0.023 ± 0.005; 7

The entries were determined on fibers that had been rested for at least 3 min before stimulation; *n* indicates the number of experiments. A dashed entry means the value was not determined or not well known. In A, the amplitude of $\Delta F/F_R$, which has been referred to the myofibrillar region of the fiber, could not be determined in all experiments because the intrinsic fluorescence of the bundle interfered with the determination of F_R (see Materials and methods); however, the time course of ΔF was well known in most fibers because of the generally large signal/noise ratio of ΔF. In B, the entries give the value of ΔF measured at either 1 or 60 s after onset of stimulation divided by ΔF_1, the peak of ΔF elicited by the first stimulated AP. In C, the entries were obtained from a least-squares fit of one of the following equations to the temporal waveform of $\Delta F(t)/\Delta F_1$: (a) with 1 AP, $\Delta F(t)/\Delta F_1 = A1 \cdot \exp(-t/\tau 1) +$ offset; (b) with 40 APs at 83 Hz, $\Delta F(t)/\Delta F_1 = A1 \cdot \exp(-t/\tau 1) + A2 \cdot \exp(-t/\tau 2) +$ offset.

(c) the kinetics of any unknown process or processes that may contribute to the small baseline offset in ΔF.

Simulation of the fluo-4 signal elicited by an AP

In Fig. 3 A, the top trace shows an averaged measurement of the $\Delta F/F_R$ signal elicited by an AP. This trace was obtained from three experiments in which $\Delta F/F_R$ appeared to be essentially free of movement artifacts, had a relatively large signal-to-noise ratio, and was recorded for 60 s after stimulation (i.e., as in Fig. 1). The amplitude of this trace was scaled to give a peak $\Delta F/F_R$ of 28.7, the mean value observed in the measurements (Table 3, A). The middle trace shows a simulation of this fluo-4 $\Delta F/F_R$ signal, performed as described in Materials and methods. The functional form used to drive the simulation (see legend of Fig. 3) corresponds to an SR Ca^{2+} release of 750 μM in ∼1 ms (Harwood et al., 2011). The 10–100% rise time, peak amplitude, and FDHM of the simulated $\Delta F/F_R$ trace are 3.2 ms, 31.8, and 15.3 ms, respectively, which are in reasonable agreement with the mean measurement values (2.6 ms, 28.7, and 15.1 ms; Table 3, A). This supports the conclusion that this simulation, including the modeled behavior of fluo-4 in the myoplasm, is reasonable. The bottom trace in Fig. 3 A shows the $\Delta[Ca^{2+}]$ waveform in the simulation. As mentioned above, it is expected that this trace is much briefer than that of the $\Delta F/F_R$ signal itself.

Fig. 3 B shows the traces in Fig. 3 A on a higher gain and a slower time base. On this slow time scale, the simulated $\Delta F/F_R$ trace is also in approximate agreement with the measured trace. The main discrepancy is that the simulated $\Delta F/F_R$ trace declines a little more rapidly than the measurement and, at 60 s after stimulation, is only slighted elevated above baseline, whereas, as noted above, the measurement reveals a more noticeable baseline offset. Better agreement between the simulation and the measurement could be obtained in simulations with a smaller concentration of Ca^{2+} pump molecules or with slower kinetics for the SR Ca^{2+} pump reactions (see Materials and methods and Fig. 10), but the agreement observed in Fig. 3 B is considered acceptable for the main issues addressed in this paper (see Discussion).

In Fig. 3 B, the time courses of the simulated $\Delta F/F_R$ trace and the simulated $\Delta[Ca^{2+}]$ trace are very similar. This is expected because, on this time scale, the simulated ΔF tracks the small and slowly changing $\Delta[Ca^{2+}]$ almost linearly.

Simulation of the fluo-4 Ca^{2+} signal elicited by a stimulus train

In Fig. 4, the top three traces in each panel show results like those in Fig. 3 except that a stimulus that mimics fiber activity during a call, 40 APs at 83 Hz, was used. The experimental $\Delta F/F_R$ signal (top trace) is an averaged response from four experiments of the type shown in Fig. 2; the conversion of the mean waveform from $\Delta F/\Delta F_1$ units to $\Delta F/F_R$ units was again made under the assumption that the mean value of $\Delta F_1/F_R$ is 28.7 (Table 3, A). The bottom trace in Fig. 4 A shows the modeled rate of SR Ca^{2+} release in this simulation. The amount of Ca^{2+} released by the first AP is 750 μM (as in Fig. 3), whereas the release amounts caused by APs after the first are substantially smaller (see legend for Fig. 4), as expected from the experimental findings mentioned in the first

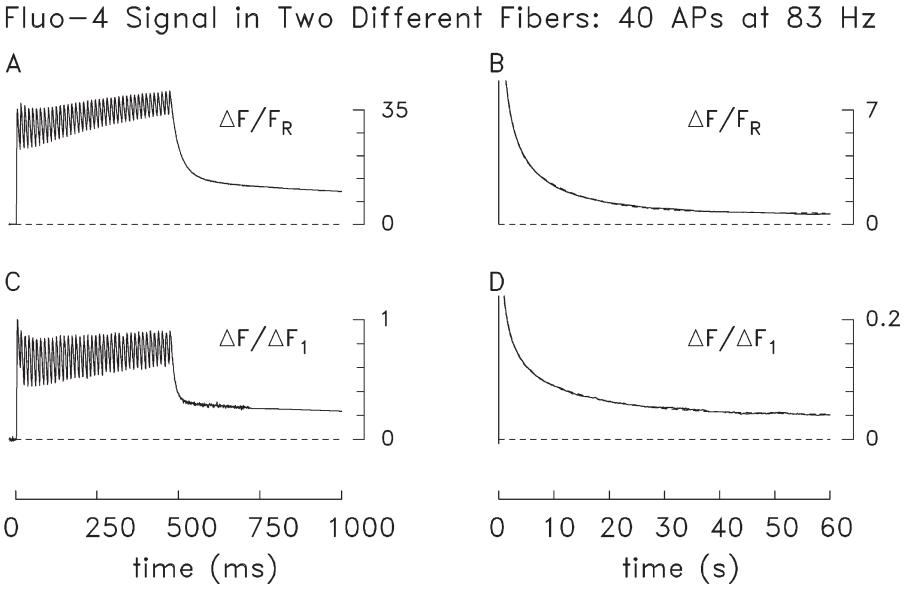

Figure 2. Examples of the fluo-4 ΔF signal elicited by a 40-AP 83-Hz stimulus train in two well-immobilized superfast swimbladder fibers (16°C). (A and C) Each trace is a single sweep corrected for a small baseline drift. In A, the trace is calibrated in units of $\Delta F/F_R$; in C, F_R was not well known and the calibration is in units of $\Delta F/F_1$, where a value of 1.0 on the ordinate corresponds to the peak amplitude of ΔF elicited by the first AP. The change in the noise level of the trace in C at ∼700 ms (see also some of the other experimental traces, e.g., in Figs. 3 B and 4 A) is explained by a data compression routine that was used during some recordings of longer-duration signals, when signal averaging reduces the noise without distorting signal kinetics. (B and D) Same traces as in A and C, respectively, but displayed on a higher gain and slower sweep speed. The declining dashed traces, which are poorly visible, show least-squares fits of the measurements between 1 and 60 s with a decaying double-exponential function to a baseline offset. The fitted parameter values in B are as follows: first exponential time constant and amplitude, 1.5 s and 4.75; second exponential time constant and amplitude, 9.9 s and 4.29; baseline offset, 0.67. The corresponding values in D are as follows: 1.7 s, 0.089, 12.9 s, 0.097, and 0.041. Fiber numbers 062713.2 (A) and 081512.2 (B).

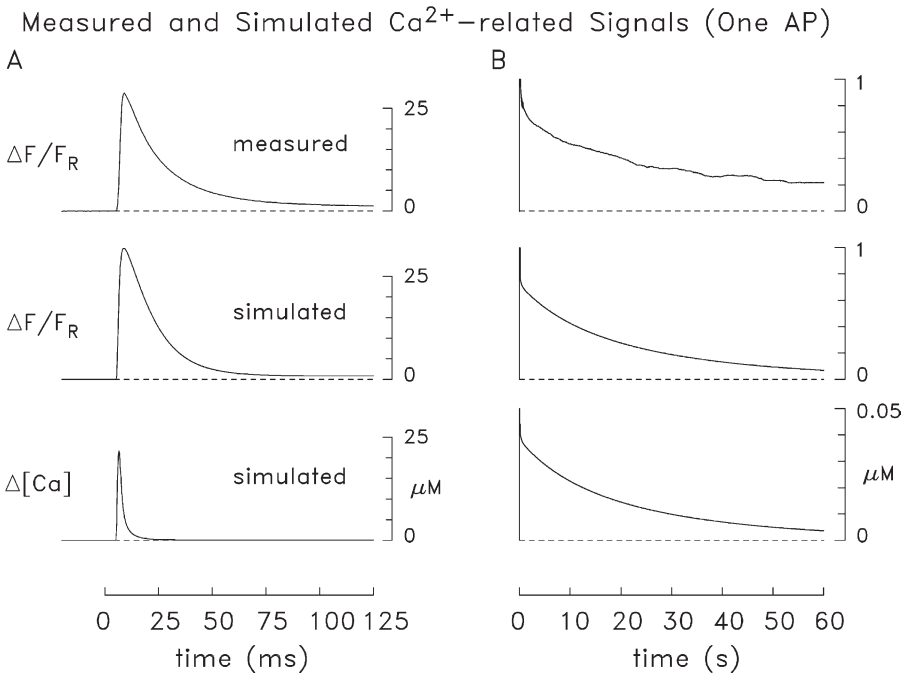

Figure 3. Measured and simulated Ca^{2+} signals in superfast swimbladder fibers stimulated by a single AP (16°C). (A) The trace at the top shows the AP-evoked $\Delta F/F_R$ signal from fluo-4, which was averaged from measurements in three well-immobilized fibers. To calculate the averaged waveform, the $\Delta F/F_R$ signal from each fiber was first normalized to a peak amplitude of 1.0 and the three waveforms were averaged; the amplitude of the latter waveform was then scaled to have a peak amplitude of 28.7, the mean peak amplitude of $\Delta F/F_R$ in Table 3 (A). The 10–100% rise time and FDHM of this signal are 2.8 ms and 16.0 ms, respectively. The middle and lower traces show $\Delta F/F_R$ and $\Delta[Ca^{2+}]$ simulated with the model. The SR Ca^{2+} release waveform (not depicted) was calculated with Eq. 1; FDHM was 1 ms, T was 5 ms, and the release amount was 750 μM. The concentration of fluo-4 in the model (50 μM) has some buffering effect on $\Delta[Ca^{2+}]$; in the absence of fluo-4, the simulated peak of $\Delta[Ca^{2+}]$ with the same release function is 24.3 μM (vs. 21.7 μM here). The amplitude of all traces has been referred to the water volume in the myofibrillar region of the fiber, i.e., excluding the fiber core (see Materials and methods). (B) Same traces as in A, but displayed on a slower sweep speed and at higher vertical gain.

section of Results. In Fig. 4, the total amount of Ca^{2+} released by the 40 APs is 6.5 mM, which is similar to the 7-mM value estimated experimentally for a 40-AP 80-Hz stimulus by the technique of recovery oxygen consumption (15°C; Harwood et al., 2011).

Although the simulated $\Delta F/F_R$ signal in Fig. 4 is in rough agreement with the measured signal, some discrepancies are apparent. In Fig. 4 A, the simulated $\Delta F/F_R$ trace decays less rapidly and less completely than the measured trace during the later APs and immediately after cessation of stimulation; in contrast, on the slow time scale of Fig. 4 B, the simulated trace returns toward baseline more rapidly and more completely than the measurement (as it does in Fig. 3). The presence of these discrepancies indicates that the myoplasmic Ca^{2+} movements estimated in these simulations, and in the simulations described below, should be considered to be approximate, not precise (see Discussion).

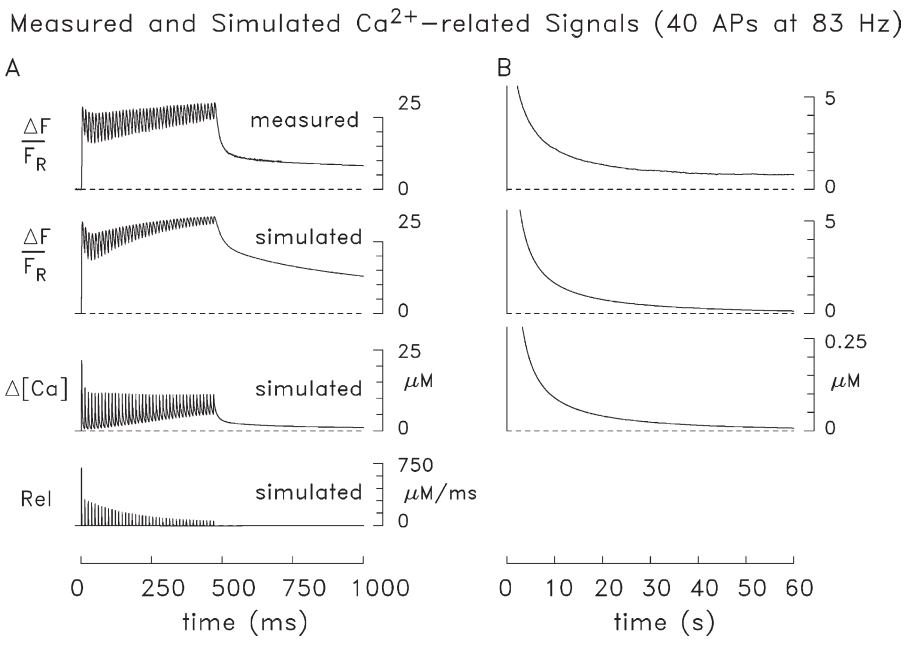

Figure 4. Comparison like that in Fig. 3 except that the stimulus was 40 APs at 83 Hz. (A and B) The experimental record (top trace) is an averaged result from four experiments in which the $\Delta F/\Delta F_1$ signal (see, e.g., Fig. 2) was well resolved and likely to be free of movement artifacts; calibration of the averaged waveform in units of $\Delta F/F_R$ is based on the value 28.7 in Table 3 (A) for the response to the first AP. The other three traces are simulated traces: $\Delta F/F_R$, $\Delta[Ca^{2+}]$, and the rate of SR Ca^{2+} release (Rel). The simulated amount of SR Ca^{2+} released by APs after the first varied from 45% to 9% of that released by the first AP. $\Delta[Ca_T]$ caused by all 40 shocks is 6,486 μM.

As observed with the experimental measurements in Fig. 2 (B and D), a decaying single-exponential function to a baseline offset does not give a good fit to the decline of the simulated fluo-4 signal in Fig. 4 between 1 and 60 s, but a decaying double-exponential function does (not depicted). The time constants and amplitudes obtained from a fit of the latter function to the simulated $\Delta F/\Delta F_1$ waveform are 1.3 s and 0.26 (first exponential), 9.6 s and 0.12 (second exponential), and 0.006 (baseline offset). These values are in rough agreement with the mean measurement values: 1.9 s, 0.12, 10.7 s, 0.11, and 0.023, respectively (Table 3, C, second column).

Details of Ca^{2+} movements during a simulated call

Fig. 5 shows additional information from the simulation of Fig. 4, including information about $\Delta[Ca^{2+}]$, $\Delta[Ca_2Trop]$, $\Delta[CaPump]$, $\Delta[CaParv]$, and the total concentration of the released Ca^{2+} that remains in the myoplasm (dashed trace labeled $\Delta[Ca_M]$, which is calculated as $\Delta[Ca_T] - \Delta[CaPumped]$). The 10-s time scale in Fig. 5 approximates the duration of a normal call (~0.5 s) plus the intercall interval (assumed here to be 9.5 s).

The Ca^{2+} release amount (6,486 μM) and the stimulus duration (480 ms) are indicated by the vertical position and length of the short horizontal line above the $\Delta[Ca_M]$ trace in Fig. 5. At 40 ms after the last stimulated AP, $[Ca^{2+}]$ is below the threshold for force generation (~3 μM), yet $\Delta[Ca_M]$ is large, 5,172 μM (0.80 of the released Ca^{2+}), of which 78% is bound to parvalbumin and 19% to the Ca^{2+} pump. At the end of the 10-s simulation period (the approximate time at which the next call in a series of calls would begin), $\Delta[Ca_M]$ is still substantial, 1,275 μM (~0.20 of the released Ca^{2+}), of which 97% is bound to parvalbumin and 2% is bound to the pump.

These results indicate that a steady-state between Ca^{2+} release and pumping would not be achieved during the first call of a repetitive series of calls. An interesting question therefore arises concerning how many calls are required, and with what adjustments, for a steady-state to be established between release and pumping during repetitive calling. Achievement of a steady-state is expected because of the positive relation between $[Ca^{2+}]$ and the rate of Ca^{2+} pumping; if any of the Ca^{2+} released during a calling cycle has not yet been fully returned to the SR, $[Ca^{2+}]$ will necessarily be elevated, thus promoting greater pumping in the next calling cycle. Also, if some Ca^{2+} that was initially in the SR still remains in the myoplasm at the start of the next cycle, the amount of Ca^{2+} released in the next cycle might be reduced (Schneider et al., 1987).

Measurement of the fluo-4 signal in response to a series of stimulus trains

To elucidate Ca^{2+} movements during repetitive calling, including how quickly Ca^{2+} release and pumping come into balance, measurements and simulations of the type shown in Figs. 4 and 5 were performed for a repetitive series of stimulus trains of 40 APs at 83 Hz. Fig. 6 A shows the fluo-4 signal measured from a fiber that was activated by four such trains initiated at intervals of 10.5 s. During each train, the $\Delta F/F_R$ signal revealed 40 individual peaks (similar to that seen in Fig. 2 A, which was measured in the same fiber); these are not resolvable in Fig. 6 A because of the compressed time scale of the plot. In all stimulus cycles, the time course of decay of ΔF after cessation of stimulation is similar to that seen in Fig. 2; thus, at the time of onset of the next cycle, ΔF is elevated above baseline. In Fig. 6 A, the four circles on the plot at the end of the cycles highlight these $\Delta F/F_R$ values, which are 1.73, 1.83, 1.88, and 1.95 (cycles 1–4, respectively).

Qualitatively similar results were seen in the two other experiments of this type. Fig. 6 (B and C) summarizes results from the three experiments. Fig. 6 B shows the mean amplitude of the fluo-4 signal at the end of each 10.5-s cycle. F_R was not well known in two of the three experiments, so, as in Fig. 6, the conversion of the measurements from $\Delta F/\Delta F_1$ units to $\Delta F/F_R$ units was made under the assumption that $\Delta F_1/F_R$ was 28.7 (Table 3, A).

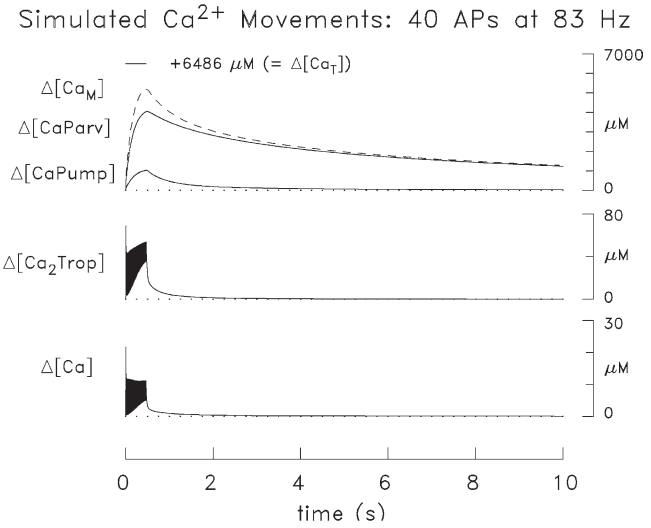

Figure 5. Additional details from the simulation in Fig. 4. $\Delta[Ca_2Trop]$ denotes the change in concentration of troponin molecules whose regulatory sites are both occupied by Ca^{2+} (maximum possible number = 106 μM; Tables 1 and 2). $\Delta[CaPump]$ and $\Delta[CaParv]$ denote the change in the concentration of Ca^{2+} ions bound to the Ca^{2+} pump and to parvalbumin. $\Delta[Ca_M]$ (dashed trace) denotes the change in the total concentration of Ca^{2+} in the myoplasm, i.e., the amount of Ca^{2+} released minus the amount of Ca^{2+} pumped ($= \Delta[Ca^{2+}] + \Delta[CaATP] + \Delta[CaTrop] + \Delta[CaParv] + \Delta[CaPump] + \Delta[CaDye]$). $\Delta[CaTrop]$ (not depicted) denotes the change in concentration of Ca^{2+} bound to all troponin regulatory sites (maximum possible number = 210.4 μM, i.e., 212 μM minus the concentration of Ca^{2+} bound at rest, 1.6 μM). The short horizontal line above the $\Delta[Ca_M]$ trace gives the stimulus duration, and the vertical displacement of this line above the dotted baseline corresponds to $\Delta[Ca_T]$ (6,486 μM; see calibration bar at right). In the absence of Ca^{2+} pumping, $\Delta[Ca_M]$ would rise to this level.

None of the mean (±SEM) values at the end of the four cycles (1.67 ± 0.17, 1.49 ± 0.32, 1.81 ± 0.17, and 1.92 ± 0.23, respectively) is significantly different from the others ($P > 0.05$). If these $\Delta F/F_R$ values are entirely caused by an elevation of $[Ca^{2+}]$, the mean of these values for the four cycles, 1.72, corresponds to a $[Ca^{2+}]$ of ~125 nM above the resting level of 30 nM (Tables 1 and 2 [E]).

Also of interest in these experiments is the relative amplitude of the ΔF signals in the four cycles during the 0.5-s periods of AP generation, when SR Ca^{2+} is being released. In the experiment of Fig. 6 A, the peaks of the $\Delta F/F_R$ signals in cycles after the first are about the same as, or slightly smaller than, the peaks of the signals in the first cycle. Because the $\Delta F/F_R$ signals in the later cycles start from values that are above baseline, ΔF (defined here as the change in fluorescence in any particular cycle above the fluorescence value at the beginning of that cycle) is slightly smaller in the later cycles than in the first cycle. This suggests that the amount of Ca^{2+} release in the later cycles was smaller than that in the first. If $\Delta F_{0.5s}$ denotes the ΔF waveform during the first 0.5 s of a cycle, the estimated amplitudes of $\Delta F_{0.5s}$ in cycles 2, 3, and 4 relative to that in the first cycle are 0.967, 0.957, and 0.942, respectively. These values were obtained from the scaling factor that gave the best least-squares fit of each of the $\Delta F_{0.5s}$ waveforms in the later cycles with the $\Delta F_{0.5s}$ waveform in the first cycle. Fig. 6 C shows the mean results for the three experiments of this type. The mean ± SEM amplitudes of $\Delta F_{0.5s}$ during the second, third, and fourth cycles relative to that in the first are 0.954 ± 0.007, 0.938 ± 0.010, and 0.921 ± 0.011, respectively ($n = 3$). These values are all significantly different from 1.0 ($P < 0.001$) but not significantly different from each other ($P > 0.05$); they indicate that the amount of SR Ca^{2+} released with a 40-AP stimulus train is probably smaller in the second and subsequent trains than in the first.

Simulation of the fluo-4 ΔF signal in response to a series of stimulus trains

To quantify the myoplasmic Ca^{2+} movements during a series of stimulus trains of the type illustrated in Fig. 6 A, simulations like that in Figs. 4 and 5 were performed but extended to four sequential stimulus cycles, each with a period of 10.5 s (which matches that of the measurements). The SR Ca^{2+} release waveform for the second and subsequent cycles was adjusted so that the simulated $\Delta F_{0.5s}$ waveform in these cycles was 0.94 times that in the first cycle (the mean of the experimental values mentioned in the last paragraph of the preceding section). This required that the amount of SR Ca^{2+} release in the second and subsequent cycles be 83.5% of that in the first cycle (5,417 and 6,486 μM, respectively).

Fig. 7 A shows the simulated $\Delta F/F_R$ signal during the four cycles of stimulation, and Fig. 7 (B and C) shows simulated values analogous to the mean measurement values in Fig. 6 (B and C). A small discrepancy between the simulations and the measurements is seen in Fig. 7 B versus Fig. 6 B. This arises because during the recovery

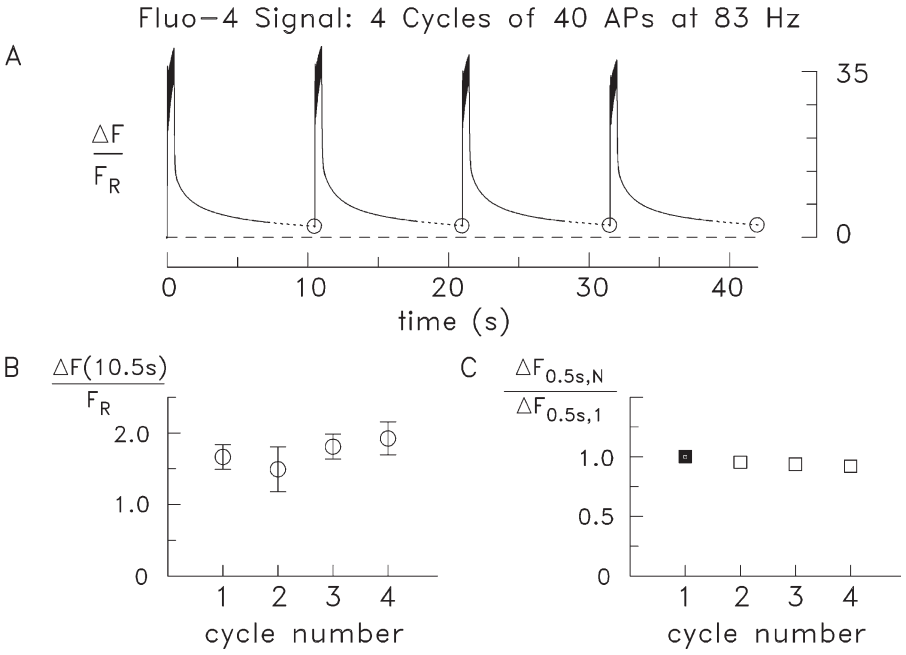

Figure 6. Properties of the measured fluo-4 $\Delta F/F_R$ signal in superfast fibers activated by consecutive stimulus trains that mimic fiber activity during cyclical calling. (A) $\Delta F/F_R$ in a fiber stimulated at 10.5-s intervals to give 40 APs at 83 Hz; F_R denotes fluo-4's fluorescence intensity measured immediately before the first stimulus train. The circles on the trace highlight the $\Delta F/F_R$ values at the end of each cycle, which are all above baseline. Each circled data point is preceded by a dashed segment that lasts 3.5 s; these segments correspond to gaps in data collection, which occurred while the preceding 7 s of data recording was being written to disk storage. Each dashed segment was obtained from the fit of a function like that described in the legend of Fig. 2 to the decay phase of the preceding $\Delta F/F_R$ signal subject to the constraint that the fitted function intersect the succeeding circled value. Fiber number 062713.2. (B) Summary data from three fibers showing estimated mean (±SEM) values of $\Delta F/F_R$ at the end of the 10.5-s stimulus cycles. (C) Mean data for the experiments of B showing $\Delta F_{0.5s,N}$, the amplitude of $\Delta F_{0.5s}$ for the different stimulus cycles (where N denotes the cycle number) divided by $\Delta F_{0.5s,1}$, the amplitude of $\Delta F_{0.5s}$ for the first cycle. $\Delta F_{0.5s}$ denotes the waveform of ΔF during the 0.5-s period of AP generation (see Measurement of the fluo-4 signal in response to a series of stimulus trains). The SEM values for the data in C were smaller than the symbol size and are not depicted.

period, the simulated $\Delta F/F_R$ waveforms return toward baseline slightly more rapidly than the measured waveforms (as in Fig. 4 B); thus, the mean amplitude of $\Delta F/F_R$ at the end of each of the four cycles is smaller in the simulations than in the measurements (mean value, 1.56 in Fig. 7 B vs. 1.72 in Fig. 6 B). Overall, the near constancy of the measurement and simulation values in Figs. 6 B and 7 B indicates that an approximate steady-state is reached beginning with the second cycle of activity.

A comparison of Fig. 7 C and Fig. 6 C shows that, as expected, the amplitudes of $\Delta F_{0.5s}$ in the second, third, and fourth cycles relative to that in the first cycle are approximately constant and similar in the simulations and the measurements. It is reasonable to conclude that a 15–20% reduction in the total amount of Ca^{2+} release occurs in the fibers during stimulus trains after the first, e.g., from ~6.5 to ~5.4 mM.

Fig. 8 shows simulated values at the ends of the four cycles for several important model variables, including Δ[CaParv] and Δ[CaPump] (Fig. 8 A) and the total amounts of SR Ca^{2+} that are released and pumped (Fig. 8 B). These plots confirm that the Ca^{2+} movements in the simulations reach a steady-state beginning with the second cycle. This occurs for two reasons: (1) the reduction in the amount of Ca^{2+} released in cycles after the first (Fig. 8 B, circle points) and (2) an enhanced rate of Ca^{2+} pumping by the SR Ca^{2+} pumps, which occurs as a result of the general elevation in $[Ca^{2+}]$ (quantified in Fig. 9). Presumably the same two factors underlie the achievement of the near steady-state observed in the fiber measurements beginning with the second cycle (Fig. 6). Overall, the general agreement between the properties of the simulated and measured fluo-4 signals supports the conclusion that the main features of the Ca^{2+} movements estimated in the simulations are approximately correct.

Kinetics of Ca^{2+} pumping during the stimulus trains

Fig. 9 gives information about Ca^{2+} pumping as a function of time in the simulations of Figs. 7 and 8. Results for the first and second simulation cycles are shown as continuous and long-dashed traces, respectively; results for the third and fourth cycles are not shown as these were essentially identical to those in the second cycle. The cumulative amount of Ca^{2+} pumped is shown in the top panel, and the estimated rate of Ca^{2+} pumping is shown in the middle panel. The traces at the bottom show a filtered version of $\Delta[Ca^{2+}]$; the points on each of these traces during the interval 0–0.5 s were obtained as mean values over each 12-ms period (the time between APs), which smooths the rapid fluctuations in $\Delta[Ca^{2+}]$ of the type seen in Fig. 4 and more clearly reveals the relation between $[Ca^{2+}]$ and Ca^{2+} pumping. The horizontal arrows at the top right point to the estimated amounts of SR Ca^{2+} release in the first and second simulation cycles (6,486 μM and 5,417 μM, respectively). The amount of Ca^{2+} pumped by the end of the second cycle, 5,404 μM, is essentially all (99.8%) of that released, whereas the amount pumped by the end of the first cycle, 5,249 μM, is only 81% of that released. As noted above, any Ca^{2+} not returned to the SR in the first cycle produces an elevation in $[Ca^{2+}]$, which favors a greater fractional return of the released Ca^{2+} in the next cycle.

The short-dashed trace in the top panel of Fig. 9 shows the simulation of Δ[CaPumped] for the hypothetical case that the amount of Ca^{2+} released in the first cycle is only 5,417 μM (i.e., the amount estimated for the second

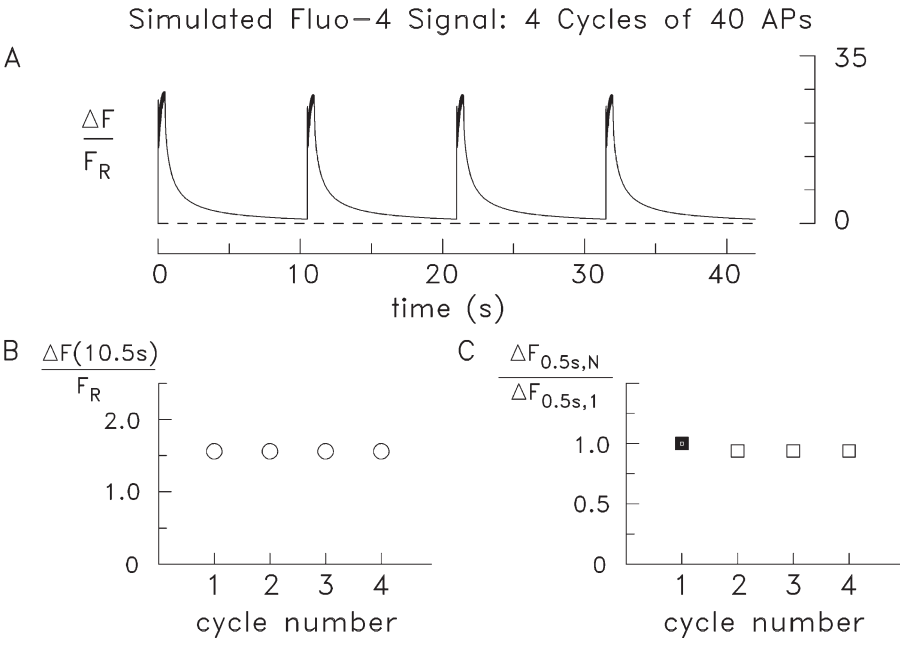

Figure 7. Simulated fluo-4 signals during four stimulus cycles of 40 APs at 83 Hz initiated at intervals of 10.5 s. (A and B) The format of the figure is identical to that in Fig. 6 for the experimental measurements. Note that (a) the measurement in Fig. 6 A is from the only fiber in which F_R (and hence $\Delta F/F_R$) could be estimated during cyclical stimulations, and (b) the amplitude of $\Delta F_1/F_R$ in this measurement, 35.2, is somewhat larger than the mean in Table 3 (A), 28.7. Thus, the simulated $\Delta F/F_R$ signal in A here is somewhat smaller than the measurement in Fig. 6 A.

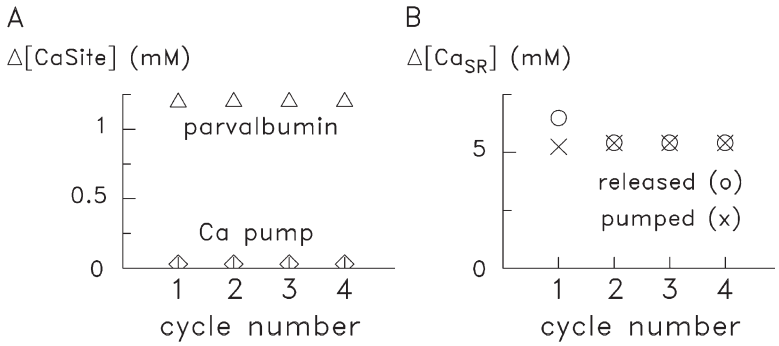

Figure 8. Changes in selected simulation values during repetitive stimulus trains. (A) Values at the end of each of the four simulation cycles for [CaParv] and [CaPump] minus their resting values. (B) The total amount of SR Ca^{2+} released and pumped in each of the four cycles (denoted generically on the ordinate as $\Delta[Ca_{SR}]$).

cycle). This trace reaches only 4,204 μM by 10.5 s, which is 78% of the release amount. Correspondingly, the short-dashed trace in the middle panel shows the rate of Ca^{2+} pumping that applies for this simulation. The peak of this trace, 2.5 μM/ms, is 67% of the peak pumping rate in the second cycle, 3.7 μM/ms. These comparisons confirm that, for a given amount of Ca^{2+} release, the elevation in $[Ca^{2+}]$ caused by activity in the first cycle increases both the peak rate and total amount of Ca^{2+} pumping in the second cycle. The short-dashed trace in the bottom panel shows (filtered) $\Delta[Ca^{2+}]$ if the amount of Ca^{2+} released in the first cycle is only 5,417 μM. A comparison of the two $\Delta[Ca^{2+}]$ traces in this panel for the two different first-cycle releases reveals that for a 20% increase in release amount (6,486 vs. 5,417 μM), the peak of (filtered) $\Delta[Ca^{2+}]$ increases by 120%. This nonlinearity occurs because the estimated amount of Ca^{2+} release for the first cycle (6,486 μM) approximately matches the available concentration of (unoccupied) Ca^{2+} buffer sites in myoplasm.

In Fig. 9, the vertical arrows in each of the three panels are located at 506 ms on the abscissa, the time at which $[Ca^{2+}]$ in the modeling has fallen below 3 μM (the approximate threshold for tension generation in swimbladder fibers). Most of the Ca^{2+} pumping occurs after this time: ~75% in all cycles. The peak rate of Ca^{2+} pumping in each stimulus train occurs at 474 ms, ~4 ms after the peak of $\Delta[Ca^{2+}]$ elicited by the last AP.

Although the peak of (filtered) $\Delta[Ca^{2+}]$ in Fig. 9 is slightly larger in the second cycle than in the first, a comparable proportional increase in the mean amplitude of (simulated) $\Delta F/F_R$ during cycle 2 compared with cycle 1 is not seen in Fig. 7 A. This occurs because $\Delta F/F_R$ is largely saturated (in all cycles) during the period of AP stimulation, i.e., 0–480 ms after the start of a cycle. A small increase in the mean of $\Delta F/F_R$ in cycle 2 versus cycle 1 does occur in Fig. 7 A during the stimulation period, consistent with the increase in the amplitude of (filtered) $\Delta[Ca^{2+}]$ during this period. This increase in mean amplitude of $\Delta F/F_R$ arises from the larger mean value of the low points in the $\Delta F/F_R$ excursions during the stimulation period, a difference which is difficult to see in the records of Fig. 7 A because of the compressed time scale.

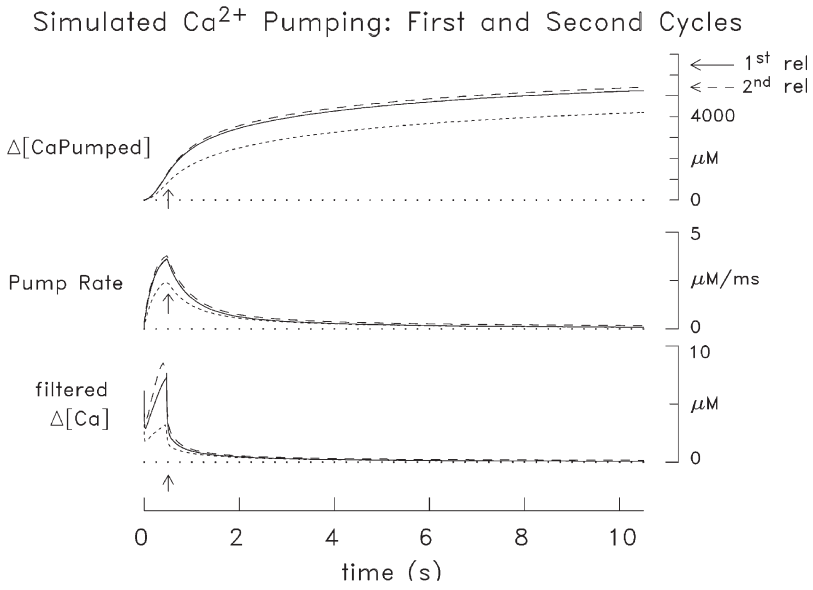

Figure 9. Comparison of simulation results in the first and second cycles of a series of 40-AP 83-Hz stimulus trains initiated at 10.5-s intervals. Zero time denotes the start of each cycle. The top and middle traces show the amount and rate of Ca^{2+} pumping; the bottom traces show a filtered version of $\Delta[Ca^{2+}]$ (see Kinetics of Ca^{2+} pumping during the stimulus trains). All traces show changes above the resting values. Results are superimposed for three different cases concerning the amount of Ca^{2+} release: 6,486 μM for the first cycle (continuous traces), 5,417 μM for the second cycle (long-dashed traces), and, hypothetically, a first-cycle release of 5,417 μM (short-dashed traces). The horizontal arrows at the top right mark the estimated actual release amounts for the first and second cycles (6,486 and 5,417 μM, respectively). The vertical arrows at the left in the three panels are positioned at time 0.51 s (i.e., 0.04 s after the last stimulated AP in each cycle), which marks the time when simulated $[Ca^{2+}]$ has fallen below 3 μM, the approximate threshold for force generation in superfast fibers. At this time, the majority of the Ca^{2+} released in each cycle remains to be returned to the SR.

At time = 3.0 s in Fig. 9, which is the time that one fourth of the amount of Ca^{2+} released in the second and subsequent cycles remains to be returned to the SR, 91% of this Ca^{2+} is bound to parvalbumin and 7% to the Ca^{2+} pumps. At the same time, $[Ca^{2+}]$ is 340 nM, and the rate of Ca^{2+} pumping is 0.40 μM/ms, which is ~11% of the peak pumping rate in this cycle. The return of the remaining released Ca^{2+} to the SR takes another 7.5 s in the second cycle (Fig. 9) and tens of seconds in the first cycle (Fig. 4). These slow returns are explained by (a) the steadily decreasing rate of Ca^{2+} pumping that applies as $[Ca^{2+}]$ approaches the resting level and (b) the substantial amount of Ca^{2+} that remains bound to parvalbumin, a high-affinity Ca^{2+} buffer. As shown in the next section, the slow return of Ca^{2+} to the SR is limited primarily by the reaction kinetics of the Ca^{2+} pump and not of parvalbumin. Because the return of the fluo-4 $\Delta F/F_R$ signal toward baseline occurs more slowly in the measurements than in the simulations, the time course of return of all the released Ca^{2+} to the SR by Ca^{2+} pumping may be even slower in the fibers than estimated in the simulations.

Simulation results with alternative choices for parameter values in the model

As noted above, some discrepancies exist between the simulated and measured fluo-4 signals, including a slightly faster and more complete return of simulated ΔF to baseline on a time scale of seconds (Figs. 3 and 4). Possible contributors to these discrepancies are errors in the choice of the parameter values in the model, not all of which are well known. To explore the potential influence of such errors, simulations were performed with at least a twofold change in several modeling parameters, including the values of resting $[Ca^{2+}]$ (see also Materials and methods), resting $[Mg^{2+}]$, the concentration of parvalbumin, the concentration of the SR Ca^{2+} pumps, and the reaction rate constants for troponin, parvalbumin, and the SR Ca^{2+} pump. None of these simulations altered the qualitative conclusions described above.

Fig. 10 compares, on two time scales, the time course of Ca^{2+} pumping associated with a 40-AP 83-Hz stimulus train in a simulation with the standard parameter values (continuous traces) and in four simulations that used alternate parameter values (dashed traces). All simulations began with the standard modeling parameters in effect (as in Figs. 4 and 5); however, at 1 s after the start of the simulation, one of the following changes was made to calculate the dashed traces: (a) the reaction rate constants for the Ca^{2+} pump were doubled (long-dashed trace above the continuous trace, labeled 1), (b) the reaction rate constants for the Ca^{2+} pump were halved (long-dashed trace below the continuous trace, labeled 1), (c) the reaction rate constants for parvalbumin were doubled (short-dashed trace above the continuous trace, labeled 2), or (d) the reaction rate constants for parvalbumin were halved (short-dashed trace below the continuous trace, labeled 2). Fig. 10 reveals that speeding/slowing the pump reactions substantially speeds/slows the final return of Ca^{2+} to the SR, whereas speeding/slowing the parvalbumin reactions has little effect on the return. It follows that the final time course with which Ca^{2+} is returned to the SR depends primarily on the kinetics of the Ca^{2+} pump and not that of parvalbumin. This conclusion appears to be quite general, as it was confirmed in several other simulations that used the method of Fig. 10 to compare the importance of the reaction kinetics of the Ca^{2+} pump and the reaction kinetics of parvalbumin. In these simulations, a several-fold change was made to one of the following variables before initiation of the five types of calculations shown in Fig. 10: (a) the resting $[Ca^{2+}]$ concentration, (b) the resting $[Mg^{2+}]$ concentration, (c) the concentration of parvalbumin, (d) the concentration of Ca^{2+} pump molecules, (e) the concentration and kinetics of troponin, and (f) the amount of SR Ca^{2+} release. In all cases, a twofold

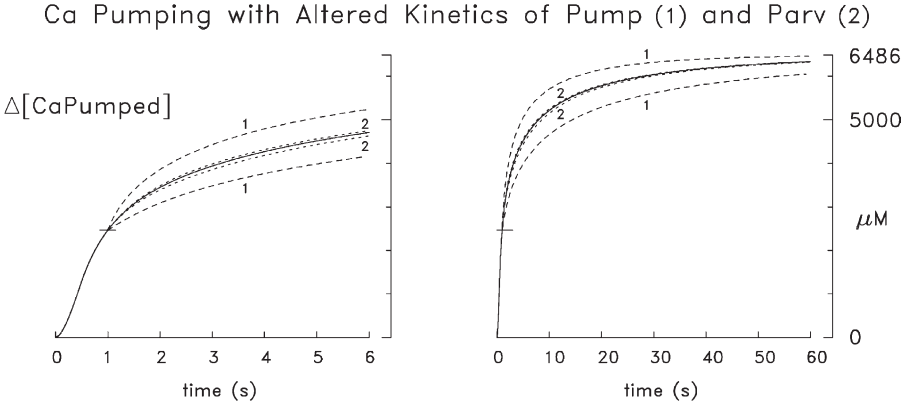

Figure 10. Simulation results for a 40-AP 83-Hz stimulus train in which several modeling parameters that affect the time course of Ca^{2+} pumping were perturbed. (left) Fast time scale. (right) Slow time scale. The continuous trace shows the amount of Ca^{2+} pumped versus time in the standard model. Each dashed trace shows the result when one of the following changes to the standard model was made at time = 1 s (where the small horizontal line crosses the curves): (a) a doubling of all reaction rate constants for the Ca^{2+} pump (long-dashed trace above the continuous curve, labeled 1), (b) a halving of all reaction rate constants for the Ca^{2+} pump (long-dashed trace below the continuous curve, labeled 1), (c) a doubling of all reaction rate constants for parvalbumin (short-dashed trace above the continuous curve, labeled 2), or (d) a halving of all reaction rate constants for parvalbumin (short-dashed trace below the continuous curve, labeled 2). The value of 6,486 μM (top of the ordinate) corresponds to the total amount of Ca^{2+} released with the 40-AP 83-Hz stimulus.

change in the kinetics of the Ca^{2+} pump reactions initiated at time = 1 s produced a much greater effect on the pumping time course than that produced by a twofold change in the kinetics of the parvalbumin reactions.

DISCUSSION

Recently, Harwood et al. (2011) estimated the amount of Ca^{2+} that is released from the SR when toadfish superfast fibers are activated by either a single AP or by a high-frequency train of APs that mimics fiber activity during a mating call. In this article, we have studied myoplasmic Ca^{2+} movements during the relaxation and recovery period after such activity by microinjecting fibers with fluo-4 and measuring the indicator's fluorescence signal in response to both single APs and high-frequency trains of APs (16°C). We have also simulated the fluo-4 $\Delta F/F_R$ signal with a single-compartment model of the myoplasmic Ca^{2+} movements, adapted to measurements with fluo-4 and extended to a time scale of seconds.

Our new measurements and simulations give an approximate picture of the principal Ca^{2+} movements that take place on a time scale of seconds after activation of swimbladder fibers by stimuli of the type that give rise to the fish's repetitive mating call, during which 6–7 mM Ca^{2+} is released from the SR in a first stimulation cycle (Figs. 4 and 5; Harwood et al., 2011). Within ∼40 ms after cessation of a 40-AP stimulus train at 83 Hz, the simulated $[Ca^{2+}]$ has fallen below the threshold for force generation, ∼3 µM; yet the estimated concentration of released Ca^{2+} that remains in the myoplasm in the myofibrillar region ($\Delta[Ca_M]$) is large, ∼5 mM, of which 78% is bound to parvalbumin and 19% is bound to the SR Ca^{2+} pumps (Fig. 5). At 10 s after onset of the stimulus train, the simulations indicate that ∼20% of the released Ca^{2+} (∼1.3 mM) has yet to be returned to the SR by Ca^{2+} pumping and $\Delta[Ca^{2+}]$ is approximately three times the resting level (Fig. 5 and associated text). Because of the elevation in $[Ca^{2+}]$, Ca^{2+} pumping in response to a second stimulus train will be elevated, so that the amount of Ca^{2+} returned to the SR during a second cycle of activity will more closely match the amount released, as shown in the measurements and simulations of Figs. 6–9.

When repetitive stimulus trains are initiated at 10.5-s intervals, release and pumping come essentially into balance by the second and subsequent stimulus cycles. The estimated amounts of Ca^{2+} released and pumped during the first stimulus cycle are 6.5 and 5.3 mM, respectively, whereas the amounts are 5.4 and 5.4 mM during the second and subsequent cycles. In terms of the fish's repetitive calling activity, the swimbladder fibers should be able to drive sound generation for many subsequent cycles, as long as the concentration of ATP and the overall energetics of the cell remain high. As reported by Harwood et al. (2011), the ATP consumption required for powering a 40-AP 80-Hz stimulus train is ∼7 mM (concentration referred to the myofibrillar water volume), of which 45–50% is for myosin, 45–50% for the SR Ca^{2+} pumps, and a few percent for the Na^+/K^+ pumps on the exterior membranes (which maintain the ion gradients that power the APs).

Discrepancies between the simulations and measurements

As noted in Results, the simulated and measured fluo-4 $\Delta F/F_R$ signals in response to an AP are in reasonable agreement on a fast time scale (Fig. 3 A). On a slow time scale, however, the simulated signal returns to baseline a little more rapidly and completely than the measurement (Fig. 3 B). A similar discrepancy is observed in response to a high-frequency stimulus train (Fig. 4 B); in contrast, immediately after a stimulus train, the simulated $\Delta F/F_R$ trace declines more slowly than the measurement (Fig. 4 A). The reason for these discrepancies is not known with certainty, but one likely contributing factor is the simplifications inherent in the use of single-compartment modeling, which considers spatially averaged Ca^{2+} movements only and changes within the myofibrillar region only. As illustrated in Fig. 10, some further small adjustment of some parameter values in the model, such as the concentrations or reaction rate constants of the Ca^{2+} pump, would give improved agreement between the simulations and the measurements on a time scale of seconds. A full exploration of these factors is more appropriately made with a multicompartment model that incorporates information about the complex anatomical features of swimbladder fibers (e.g., as described by Appelt et al. [1991]). Overall, the current simulations with the single-compartment model appear to give a reasonable working picture of the myoplasmic Ca^{2+} movements during the recovery periods after activity.

Influence of a large parvalbumin concentration on the time course of Ca^{2+} pumping

In toadfish superfast swimbladder fibers, the myoplasmic concentration of metal-binding sites on parvalbumin is in the millimolar range (5.34 mM, Table 1). A large concentration of such high-affinity, slowly reacting Ca^{2+}-binding sites (which also bind Mg^{2+}) assists the SR Ca^{2+} pumps in lowering $[Ca^{2+}]$ near or below the threshold for force generation after cessation of SR Ca^{2+} release, thus speeding contractile relaxation (Briggs, 1975; Gerday and Gillis, 1976; Gillis et al., 1982). As illustrated in the measurements and modeling of this article, this action of parvalbumin is also associated with a slow return of Ca^{2+} to the SR after the excitation-contraction coupling period is over. Because the binding of Ca^{2+} to parvalbumin results in a lower level of $[Ca^{2+}]$ than would otherwise occur, a slower rate of Ca^{2+} pumping by the SR Ca^{2+} pumps ensues; therefore, the time required to return the released Ca^{2+} to the SR is necessarily prolonged by the presence of parvalbumin. If a rested swimbladder fiber is stimulated

by either a single AP or one high-frequency train of APs, the results indicate that it takes tens of seconds for the SR to resequester a large fraction of the released Ca^{2+} (16°C; Figs. 1–4 and Fig. 9, top, continuous trace). The slow return of Ca^{2+} to the SR is rate limited primarily by the reaction rate constants of the SR Ca^{2+} pump, not those of parvalbumin (Fig. 10 and associated text).

Other vertebrate fibers also contain millimolar concentrations of metal-binding sites on parvalbumin. In frog twitch fibers (Hou et al., 1991) and mouse fast-twitch fibers of the type IIb category (Heizmann et al., 1982; Ecob-Prince and Leberer, 1989), the concentration of parvalbumin is ∼25–30% of that in swimbladder fibers. Because the concentration of SR Ca^{2+} pumps in these fibers is ∼10–15% of that in superfast swimbladder fibers (e.g., Ferguson and Franzini-Armstrong, 1988; Appelt et al., 1991), the ratio of Ca^{2+} pump molecules to parvalbumin molecules is about half that in swimbladder fibers. Thus, in these frog and mouse fibers, as in swimbladder fibers, the resequestration of the SR Ca^{2+} released during excitation-contraction coupling is expected to be completed on a time scale of many seconds, with the slow turnover rate of the SR Ca^{2+} pumps at low $[Ca^{2+}]$ again likely to be the rate-limiting process (rather than the reaction kinetics of parvalbumin, as has sometimes been suggested; e.g., Hou et al., 1992). Indeed, in experiments with fluo-3 and fluo-4 on frog twitch fibers and on mouse fast-twitch fibers from extensor digitorum longus (EDL) muscles, (a) the return of the fluo $\Delta F/F_R$ signal toward baseline also takes tens of seconds in response to either a single AP or a high-frequency train of APs, and (b) calculations like those presented in this paper (with appropriate adjustment of the parameter values in the model) indicate that these slowly declining signals are again rate limited by Ca^{2+} pumping, which continues for many seconds before Ca^{2+} is cleared from parvalbumin and fully returned to the SR (16°C; unpublished data). In frog fibers injected with fura-2, another high-affinity Ca^{2+} indicator, a slow decline of the indicator's fluorescence signal elicited by APs is also observed on a 60-s time scale, consistent with a slow decline of $[Ca^{2+}]$ (18°C; Suda and Kurihara, 1991). Conversely, in fibers from mouse soleus muscle (a slow-twitch muscle which has little or no parvalbumin), the return of the fluo-4 signal toward baseline is about sixfold faster than that in frog twitch fibers or mouse fast-twitch fibers (16°C; Baylor, S.M., and S. Hollingworth. 2013. Annual Meeting of the Biophysical Society. Abstr. 1498).

Our inference that the return of released Ca^{2+} to the SR in mouse EDL fibers stimulated by an AP requires many seconds of Ca^{2+} pumping is at odds with a recent study in which the return of SR Ca^{2+} was estimated by means of heat measurements (Barclay, 2012). The latter study reported that the activity-related change in heat in EDL fibers was essentially complete by 2 s after an AP (20°C) and concluded that 97% of the released Ca^{2+} had been returned to the SR by the 2-s time point. An alternative explanation of the finding of no heat change after 2 s is that the heat generated as the result of turnover of the Ca^{2+} pumps is approximately matched by the heat absorbed when Ca^{2+} dissociates from parvalbumin (Tanokura, 1990; Barclay, 2012). These two processes might then proceed concurrently for many seconds without a readily resolvable contribution to the heat measurements.

Summary of design features for repetitive calling

As noted in Table 1, swimbladder fibers have a troponin isoform with a low affinity for Ca^{2+} (estimated $K_{d,Ca}$ = 3.9 µM), a large concentration of parvalbumin, and a large concentration of SR Ca^{2+} pumps. As confirmed in this article, these features permit $\Delta[Ca^{2+}]$ to fall near or below the contractile threshold after each AP in a stimulus train of the type that gives rise to the fish's mating call. Once the stimulus is over, $[Ca^{2+}]$ falls quickly to a level where there is little or no activation of the myosin cross-bridges, yet $[Ca^{2+}]$ remains sufficiently elevated above the resting level to permit Ca^{2+} pumping at rates substantially above the resting pump rate. In extremes, Ca^{2+} pumping in swimbladder fibers can even occur with >50% of the maximum pumping activity at a $[Ca^{2+}]$ level that produces almost no activation of the myofilaments (e.g., 1 µM; see Fig. 3 B of Young et al. [2003]). These and other design features, including a myosin isoform with a fast detachment rate constant (Rome, 2006), underlie the ability of the swimbladder fibers to generate intermittent high-frequency bursts of twitches for long periods, as required for the fish's calling behavior during mating.

This work was supported by a grant to S.M. Baylor from the National Institutes of Health (GM 086167) and a grant to L.C. Rome from the National Science Foundation (IOS-1145981).

The authors declare no competing financial interests.

Richard L. Moss served as editor.

Submitted: 1 January 2014
Accepted: 24 March 2014

REFERENCES

Appelt, D., V. Shen, and C. Franzini-Armstrong. 1991. Quantitation of Ca ATPase, feet and mitochondria in superfast muscle fibres from the toadfish, *Opsanus tau*. *J. Muscle Res. Cell Motil.* 12:543–552. http://dx.doi.org/10.1007/BF01738442

Barclay, C.J. 2012. Quantifying Ca^{2+} release and inactivation of Ca^{2+} release in fast- and slow-twitch muscles. *J. Physiol.* 590:6199–6212. http://dx.doi.org/10.1113/jphysiol.2012.242073

Baylor, S.M., and S. Hollingworth. 1998. Model of sarcomeric Ca^{2+} movements, including ATP Ca^{2+} binding and diffusion, during activation of frog skeletal muscle. *J. Gen. Physiol.* 112:297–316. http://dx.doi.org/10.1085/jgp.112.3.297

Baylor, S.M., and S. Hollingworth. 2007. Simulation of Ca^{2+} movements within the sarcomere of fast-twitch mouse fibers stimulated by action potentials. *J. Gen. Physiol.* 130:283–302. http://dx.doi.org/10.1085/jgp.200709827

Baylor, S.M., and S. Hollingworth. 2011. Calcium indicators and calcium signalling in skeletal muscle fibres during excitation-contraction coupling. *Prog. Biophys. Mol. Biol.* 105:162–179. http://dx.doi.org/10.1016/j.pbiomolbio.2010.06.001

Baylor, S.M., S. Hollingworth, and W.K. Chandler. 2002. Comparison of simulated and measured calcium sparks in intact skeletal muscle fibers of the frog. *J. Gen. Physiol.* 120:349–368. http://dx.doi.org/10.1085/jgp.20028620

Briggs, N. 1975. Identification of the soluble relaxing factor as a parvalbumin. *Fed. Proc.* 34:540.

Cheung, A., J.A. Dantzig, S. Hollingworth, S.M. Baylor, Y.E. Goldman, T.J. Mitchison, and A.F. Straight. 2002. A small-molecule inhibitor of skeletal muscle myosin II. *Nat. Cell Biol.* 4:83–88. http://dx.doi.org/10.1038/ncb734

Ecob-Prince, M.S., and E. Leberer. 1989. Parvalbumin in mouse muscle in vivo and in vitro. *Differentiation.* 40:10–16. http://dx.doi.org/10.1111/j.1432-0436.1989.tb00808.x

Elemans, C.P.H., A.F. Mensinger, and L.C. Rome. 2014. Vocal production complexity correlates with neural instructions in the oyster toadfish (*Opsanus tau*). *J. Exp. Biol.* http://dx.doi.org/10.1242/jeb.097444

Feher, J.J., T.D. Waybright, and M.L. Fine. 1998. Comparison of sarcoplasmic reticulum capabilities in toadfish (*Opsanus tau*) sonic muscle and rat fast twitch muscle. *J. Muscle Res. Cell Motil.* 19:661–674. http://dx.doi.org/10.1023/A:1005333215172

Felder, E., and C. Franzini-Armstrong. 2002. Type 3 ryanodine receptors of skeletal muscle are segregated in a parajunctional position. *Proc. Natl. Acad. Sci. USA.* 99:1695–1700. http://dx.doi.org/10.1073/pnas.032657599

Ferguson, D.G., and C. Franzini-Armstrong. 1988. The Ca^{2+} ATPase content of slow and fast twitch fibers of guinea pig. *Muscle Nerve.* 11:561–570. http://dx.doi.org/10.1002/mus.880110607

Gerday, C., and J.M. Gillis. 1976. Proceedings: The possible role of parvalbumins in the control of contraction. *J. Physiol.* 258:96P–97P.

Gillis, J.M., D. Thomason, J. Lefèvre, and R.H. Kretsinger. 1982. Parvalbumins and muscle relaxation: a computer simulation study. *J. Muscle Res. Cell Motil.* 3:377–398. http://dx.doi.org/10.1007/BF00712090

Harkins, A.B., N. Kurebayashi, and S.M. Baylor. 1993. Resting myoplasmic free calcium in frog skeletal muscle fibers estimated with fluo-3. *Biophys. J.* 65:865–881. http://dx.doi.org/10.1016/S0006-3495(93)81112-3

Harwood, C.L., I.S. Young, B.A. Tikunov, S. Hollingworth, S.M. Baylor, and L.C. Rome. 2011. Paying the piper: the cost of Ca^{2+} pumping during the mating call of toadfish. *J. Physiol.* 589:5467–5484. http://dx.doi.org/10.1113/jphysiol.2011.211979

Heizmann, C.W., M.W. Berchtold, and A.M. Rowlerson. 1982. Correlation of parvalbumin concentration with relaxation speed in mammalian muscles. *Proc. Natl. Acad. Sci. USA.* 79:7243–7247. http://dx.doi.org/10.1073/pnas.79.23.7243

Hollingworth, S., and S.M. Baylor. 2013. Comparison of myoplasmic calcium movements during excitation-contraction coupling in frog twitch and mouse fast-twitch muscle fibers. *J. Gen. Physiol.* 141:567–583. http://dx.doi.org/10.1085/jgp.201310961

Hollingworth, S., C. Soeller, S.M. Baylor, and M.B. Cannell. 2000. Sarcomeric Ca^{2+} gradients during activation of frog skeletal muscle fibres imaged with confocal and two-photon microscopy. *J. Physiol.* 526:551–560. http://dx.doi.org/10.1111/j.1469-7793.2000.t01-1-00551.x

Hollingworth, S., J. Peet, W.K. Chandler, and S.M. Baylor. 2001. Calcium sparks in intact skeletal muscle fibers of the frog. *J. Gen. Physiol.* 118:653–678. http://dx.doi.org/10.1085/jgp.118.6.653

Hollingworth, S., M.M. Kim, and S.M. Baylor. 2012. Measurement and simulation of myoplasmic calcium transients in mouse slow-twitch muscle fibres. *J. Physiol.* 590:575–594. http://dx.doi.org/10.1113/jphysiol.2011.220780

Hou, T.-T., J.D. Johnson, and J.A. Rall. 1991. Parvalbumin content and Ca^{2+} and Mg^{2+} dissociation rates correlated with changes in relaxation rate of frog muscle fibres. *J. Physiol.* 441:285–304.

Hou, T.-T., J.D. Johnson, and J.A. Rall. 1992. Effect of temperature on relaxation rate and Ca^{2+}, Mg^{2+} dissociation rates from parvalbumin of frog muscle fibres. *J. Physiol.* 449:399–410.

Peinelt, C., and H.-J. Apell. 2002. Kinetics of the Ca^{2+}, H^{+}, and Mg^{2+} interaction with the ion-binding sites of the SR Ca-ATPase. *Biophys. J.* 82:170–181. http://dx.doi.org/10.1016/S0006-3495(02)75384-8

Rome, L.C. 2006. Design and function of superfast muscles: new insights into the physiology of skeletal muscle. *Annu. Rev. Physiol.* 68:193–221. http://dx.doi.org/10.1146/annurev.physiol.68.040104.105418

Rome, L.C., D.A. Syme, S. Hollingworth, S.L. Lindstedt, and S.M. Baylor. 1996. The whistle and the rattle: the design of sound producing muscles. *Proc. Natl. Acad. Sci. USA.* 93:8095–8100. http://dx.doi.org/10.1073/pnas.93.15.8095

Schneider, M.F., B.J. Simon, and G. Szucs. 1987. Depletion of calcium from the sarcoplasmic reticulum during calcium release in frog skeletal muscle. *J. Physiol.* 392:167–192.

Suda, N., and S. Kurihara. 1991. Intracellular calcium signals measured with fura-2 and aequorin in frog skeletal muscle fibers. *Jpn. J. Physiol.* 41:277–295. http://dx.doi.org/10.2170/jjphysiol.41.277

Tanokura, M. 1990. Heat capacity and entropy changes of the major isotype of the toad (*Bufo*) parvalbumin induced by calcium binding. *Eur. J. Biochem.* 188:23–28. http://dx.doi.org/10.1111/j.1432-1033.1990.tb15366.x

Woodruff, M.L., A.P. Sampath, H.R. Matthews, N.V. Krasnoperova, J. Lem, and G.L. Fain. 2002. Measurement of cytoplasmic calcium concentration in the rods of wild-type and transducin knockout mice. *J. Physiol.* 542:843–854. http://dx.doi.org/10.1113/jphysiol.2001.013987

Young, I.S., C.L. Harwood, and L.C. Rome. 2003. Cross-bridge blocker BTS permits direct measurement of SR Ca^{2+} pump ATP utilization in toadfish swimbladder muscle fibers. *Am. J. Physiol. Cell Physiol.* 285:C781–C787. http://dx.doi.org/10.1152/ajpcell.00025.2003